International Symposium of Research Students on Material Science and Engineering
December 20-22, 2004, Chennai, India
Department of Metallurgical and Materials Engineering, Indian Institute of Technology Madras

THE EFFECT OF PRECIPITATE DISTRIBUTIONS ON HSLA GRAIN STRUCTURES

D. Chakrabarti, C. L. Davis and M. Strangwood
The University of Birmingham, Department of Metallurgy and Materials, Edgbaston, Birmingham, B15 2TT UK

ABSTRACT

Bimodal grain size distributions were found in continuously cast slab and thermomechanical controlled rolled (TMCR) samples of Nb-microalloyed steel. Scanning electron microscopy (SEM) revealed inhomogeneous distributions of Al- and Nb-containing precipitates, which were found to pin prior austenite grain boundaries during reheating. Fine austenite grain sizes were associated with areas having a higher number density of these precipitates, which correlated with interdendritic regions. The formation of a bimodal grain structure after reheating and rolling could therefore be attributed to the inhomogeneous precipitate distribution, which originates from segregation during continuous casting and is modified during reheating and rolling.

Keywords: Microalloyed steel, precipitate distribution, segregation, grain-size distribution

1. INTRODUCTION

Over the last thirty years, high strength low alloy (HSLA) steels containing microalloying elements such as Ti, Nb and V have become widely used in construction and pipeline applications. Thermomechanical controlled rolling (TMCR) has been introduced to reduce the processing cost and to improve both the strength and toughness of microalloyed steels by grain refinement, in comparison to commercial hot rolling, through incorporation of hold periods in the rolling schedule and low finish rolling temperatures (typically ~ 750-850°C).

Grain refinement results from the inhibition of austenite grain growth during reheating and retardation of both static and dynamic recrystallization of austenite during TMCR by the fine microalloy (Nb, V and Ti) carbide and nitride precipitates [1]. This results in a fine final grain size [2-4]. Nb is known to be the most effective microalloy element to achieve grain refinement, but will tend to partition to interdendritic regions during solidification along with carbon and nitrogen [5, 6], which can lead to inhomogeneous precipitation of C,N-rich particles on solidification [7]. The inhomogeneous distribution can lead to a variation in local grain boundary (Zener) pinning [8], as well as changing the degree and rate of particle dissolution during reheating. Localized partial dissolution and inhomogeneous distribution of microalloy precipitates may lead to inhomogeneous grain growth during reheating [7, 9-11]. During rolling, the combination of inhomogeneous prior austenite grain size and particle distributions; the latter also occurring during cooling and deformation [12, 13] will affect the local recovery and recrystallization processes and hence the final ferrite grain size. Thus, a variation in prior austenite grain size can result in inhomogeneous ferrite grain size distribution upon rolling. In recent years a variation in grain size, particularly a bimodal ferrite grain size distribution has been observed in some TMCR Nb and Nb-V microalloyed steel plates, with abnormally large ferrite grains present in the matrix of smaller grains, in a typically banded ferrite-pearlite microstructure [14,15].

All stages of processing, casting, reheating and rolling, can contribute to the final microstructure and so it is necessary to understand the effect of commercial reheating of as-cast steel slabs on the formation of bimodal ferrite grain structure in the final TMCR plates. This is covered in this paper through the study of the sequential changes taking place in microstructural features and precipitate distribution during the commercial processing stages (starting from as-cast steel to reheated and rolled steel).

2. MATERIALS AND EXPERIMENTAL TECHNIQUE

Two as-continuously cast (290 mm thick and 1800 mm wide) low-carbon microalloyed steel slabs, Table 2.1, with the same continuous casting process parameters were investigated. A rolled plate sample (44 mm thickness) from the ¼ width position of a single steel cast, Table 2.1, was also supplied. The plate rolling schedule was based on reheating to 1150-1200°C and rolling to a 3:1 < 810°C double hold TMCR schedule with the aim finish rolling temperature (FRT) being 700-720°C. The total rolling reduction was ~ 5:1.

10×10×10-mm samples were cut from the quarter-thickness position of as-cast slabs, sealed in evacuated silica tubing and subjected to re-heating and re-heating + holding heat treatments, Table 2.2. Longitudinal sections of as-cast and rolled steels were mounted in bakelite, polished to a 0.05 μm SiO_2 finish and etched in 2%-nital or saturated aqueous picric acid solution at 60°C (to reveal prior austenite grain structure). These specimens were examined using a KS400 image analyser to quantify cast, rolled and heat treated structures (secondary dendrite arm spacing (SDAS), coarse (> 1 μm) inclusions, grain size - equivalent circle diameter (ECD) – and aspect ratio distributions, second phase (pearlite or bainite) fraction and the centre-to-centre distance between two neighbouring coarse-to-coarse and fine-to-fine grain bands, in bimodal grain structures). About five hundred grains were measured for each grain size distribution. Inclusions finer than 1 μm and precipitates in the as-cast and reheated steels were characterised in a Jeol 6060 scanning electron microscope (SEM) and by Philips XL-30 FEG environmental SEM, equipped with Oxford Inca EDS facility.

3. RESULTS AND DISCUSSION

3.1 Microstructure and precipitates of as-cast slabs

The microstructures of sub-surface, quarter-thickness and mid-thickness positions of continuous cast slab 1 are shown in Fig. 3.1 and are similar in slab 2. The number averaged SDAS and ferrite grain size values measured at several through-thickness locations for both slabs, Table 3.1, indicate that the finest SDAS and ferrite grain sizes are near the top-surface, which experienced the highest cooling rates. Moving towards the slab centre, the cooling rate decreases and there is an increase in both SDAS and ferrite grain size. The distributions of ferrite grain sizes, Fig. 3.2, however, show a bimodal distribution with two peaks for area fraction as a function of ferrite grain size in the sub-surface (20 mm) position. The mid-thickness position is characterised by a single peak. The skewed grain size distribution in the sub-surface position of as-cast slab indicates that a bimodal distribution may start during casting.

An inhomogeneous distribution of precipitates was found on the polished surface of both the as-cast slabs, Fig.3.3, with the precipitate-rich regions (indicated by A, B & C) separated by regions of low precipitate density. The separation of precipitate-rich regions was consistent with the distances between interdendritic regions as the centre-to-centre distances between regions, such as A, B and C, at quarter thickness position of both the slabs lie between 200 and 250 μm, i.e. similar to SDAS at that position of the slabs (211 μm for slab-1 and 198 μm for slab-2). SEM imaging of the inhomogeneous nature of precipitate distributions, Fig. 3.4, indicates that larger ferrite grains are associated with precipitate-depleted regions, whilst precipitate-rich regions generally exhibited a finer grain size. Energy dispersive spectroscopy,

EDS, analysis on the cluster of precipitates in high precipitate regions, Fig.3.4(b), and the isolated precipitates on the low precipitate regions revealed that the inhomogeneously distributed precipitates were, irregular AlN, spherical Nb(C,N) and complex (Al,Nb)(C,N), with sizes ranging from 10 nm to 150 nm. Al- and Nb-rich precipitates were often clustered together in regions of high precipitate number densities, whilst, Ti-rich precipitates, of size 50-200 nm, were generally found associated with Nb-rich particles. The presence of these particle phases agreed with Thermo-Calc predictions for precipitation sequences in these compositions [16].

The extent of inhomogeneity in the distribution of Al- and Nb-rich precipitates has been quantified in terms of the difference between maximum and minimum precipitate area density and interparticle spcing, Table 3.2. These show that average precipitate density and the inhomogenity of distribution both increase with increasing distance from the slab surface. The increase in average precipitate density could be due to the advancing solidification front driving the fine precipitates towards the slab centre, whilst the delay in complete solidification with increasing distance from slab surface can give rise to higher segregation and hence, a more inhomogeneous precipitate distribution in the interdendritic regions towards mid-thickness.

3.2 Microstructure and precipitates of the reheated samples

Reheating samples from both slabs for 1 hour at temperatures between 1075 and 1150°C resulted in a bimodal prior austenite grain structure (shown by water quenching and tempering), with fine and coarse grain regions in the distribution peaking at 40-60 and 240-260 μm respectively, Fig. 3.5 and Fig. 3.6(a). Average distance between two neighbouring fine grain regions, measured normal to the length of the fine grain bands, is 247 μm (±45 μm), which is similar to the average SDAS value of 211 μm for the quarter thickness position of as-cast slab 1. The degree of bimodality decreased as reheating temperature increased and disappeared for reheating at 1225 °C when a more homogeneous, but coarse grain size resulted, Fig. 3.6(b).

SEM-EDS study of particles present at prior austenite grain boundaries in coarse and fine grained regions indicated approximately twice as many particles per unit length of boundary (0.15 – 0.16 μm^{-1}) for fine (<20 μm diameter) than for coarse (>20 μm diameter) grains (0.05 – 0.08 μm^{-1}) reinforcing the link between fine grain size and precipitate-rich regions. The majority of precipitates pinning the grain boundaries were found to be AlN, Nb(C,N) or Al-Nb(C,N) complex precipitates with a small number of fine MnS/ CuS inclusions and Nb,Ti-rich precipitates also present. The majority of precipitates pinning austenite grain boundaries were Al/Nb/Al-Nb-rich particles (60 – 80 % of those present), but the number of these actually present for reheating to 1225 °C is very low, which is consistent with the large grain growth that occurs as almost full dissolution of pinning particles takes place; Thermo-Calc predicts dissolution in the temperature range 1131 – 1165 °C. Therefore, increase in reheating temperature from 1075°C to 1150°C results in partial dissolution of the Al-, Nb-rich precipitates pinning grain boundaries of slab 1, the extent of which would be expected to vary between precipitate-rich and precipitate-lean regions. Thus a bimodal grain distribution would be expected. Complete dissolution at 1225 °C would be consistent with a larger and more uniform grain size.

3.3 Isothermally transformed structure

A 700 °C hold without deformation resulted in a ferrite-pearlite structure, Fig. 3.7(a), with regions of coarse ferrite grains lying between regions of finer ones. The bimodal nature of the microstructure is represented by the grain size (number frequency and area fraction) distribution plot, Fig. 3.7(b). On cooling or isothermal holding ferrite nucleates at the prior-austenite grain boundaries and, due to the lack of available nucleation sites in abnormally large austenite grains, the ferrite is expected to grow large to a larger size before impingement

in coarse prior austenite grain regions than in finer. The average centre-to-centre distance between neighbouring coarse grain regions in isothermally transformed steel (232 ± 43 μm) correlates with that for the prior-austenite structure (247 ± 45 μm), which also supports this hypothesis and suggests a dependence on the average-SDAS of the as-cast steel.

3.4 Microstructural characterization of rolled plate

The microstructures of the commercial TMCR-plate were studied through thickness from the top surface (0 mm) to mid-thickness (22 mm from the top rolling surface). At the quarter-thickness position the microstructure is composed, Fig. 3.8(a), of patches of coarse ferrite grains in a banded fine ferrite and pearlite matrix. The TMCR-plate exhibits a bimodal distribution of ferrite grains, Fig. 3.8(b), which peaks at the 6-9 μm and at 18-21 μm size ranges. The average (ECD) ferrite grain size is found to increase from the sub-surface towards the mid-thickness, Table 3.3. The faster cooling of the rolled plates compared with the cast slab has resulted in the presence of ~1 % bainite along with ~10 % pearlite as the second phase. Average centre-to-centre distance between two neighbouring fine ferrite grain bands, in a normal direction to the bands, at quarter thickness position of rolled plate was found to be, 46 μm (±9 μm), which is approximately one fifth of the SDAS value for the slab at this position, 211 μm (±36 μm), suggesting that the influence of cast structure and segregation persists through rolling deformation.

3.5 Summary

Inhomogeneous distributions of Al- and Nb-rich precipitates have been found in continuous cast slabs with the precipitate-rich regions being associated with the interdendritic regions and separated from each other by a distance similar to the average secondary dendritic arm spacing (SDAS). Similar composition precipitates were found to pin the prior austenite grain boundaries in reheated steel which exhibited a bimodal austenite grain size distribution. Bimodality was also observed in samples which had been reheated with an isothermal hold and in rolled plate. In all cases, the fine-to-fine grain band spacing could be related to the SDAS values. Uniform grain structure was only observed when almost complete dissolution of these particles occurred, i.e. reheating to 1225 °C.

The above findings suggest that the inhomogeneous precipitate distribution could be the result of segregation of Al and Nb to the interdendritic regions during solidification as the steel is continuously cast, Fig.3.9 (a). The presence of increased levels of Al, C, N and Nb in interdendritic regions will increase the precipitation of Al- and Nb-rich carbo-nitrides (particularly at grain boundaries, [17]), which also have a high solvus temperature due to the local composition. By comparison, any precipitates formed in precipitate-lean regions will form in material with low solute levels and so have a low solvus temperature. The high solvus precipitates undergo less dissolution and coarsening in the precipitate-rich interdendritic regions, whereas low solvus precipitates dissolve and coarsen more easily, Fig.3.9 (b). This can create a local variation in the volume fraction and size of precipitates effective to pin austenite grain boundaries during reheating through Zener drag, which varies as [18, 19]:

$$F_P \alpha \frac{\gamma . f}{r}$$

Where, F_P is the maximum pinning force, f is the volume fraction of precipitate, r is the average precipitate radius and γ is the grain boundary energy per unit area.
As a result the effective pinning force will be higher at the precipitate-rich, interdendritic regions, which retain a higher volume fraction of particles, f, resulting in a finer grain size during and after reheating, Fig.3.9 (c). Grains in the low precipitate-lean regions would be expected to grow to a large size. Difference in grain size upon reheating can be carried forward through the rolling stages and finally result in a bimodal distribution of ferrite grains in rolled plate.

4. CONCLUSIONS AND FUTURE WORK

- Interdendritic segregation during casting can generate an inhomogeneous precipitate distribution in as-cast slab.
- The bimodal distribution may start during casting and develop during reheating and rolling.
- Inhomogeneous precipitate distributions present during reheating can create a difference in precipitate pinning force between different regions of the steel, and can result in a strengthening of the bimodality of grain structure.
- Reheating temperature has an effect on bimodality of steel with complete dissolution at high reheating temperatures giving a uniform, but large grain size.

The present investigation has identified a working hypothesis for the formation of bimodal grain size distributions in continuously cast, reheated and rolled steels. This will need to be extended to a larger matrix of compositions and thermomechanical treatments in order to verify this mechanism and identify those conditions leading to significant bimodality. Mechanical property testing is also needed to quantify the effects of grain size distribution on strength and toughness.

5. REFERENCES

1. T. Gladman; The Physical Metallurgy of Microalloyed Steels, Book 615, The Institute of Materials, (1997).
2. J. A. Rodrigues, J. R. Dermonde, Mat. Sci. and Tech., Vol.1, p.29 (1985).
3. I. Tamura, C. Ouchi, T. Tanaka, H. Sekine, 'Thermo-mechanical Processing of HSLA Steels', Butterworths, Stoneham, MA (1988).
4. J. R. Wilcox, R. W. K. Honeycombe, Mat. Sci. and Tech., Vol.3, p.849, (1987).
5. G. Tither and Z. Shauhau, JOM, (The Minerals, Metals and Materials Society), Vol.44, p.115, (1992).
6. Z. Chen, M. H. Loretto, R. C. Cochrane, Mat. Sci. and Tech., Vol.3, p.836, (1987).
7. C.L. Davis, M. Strangwood; Journal of Materials Science, Vol.37, p.1083-1090, (2002).
8. C. Zener, quoted in C.S. Smith, Trans. AIME, Vol.175, p.47, (1948).
9. L.J. Cuddy, J.C. Raley; Metall. Trans., Vol.14A, p.1989-1995, (1983).
10. E.J. Palmiere, C.I. Garcia, A.J. DeArdo; Metall. Trans., Vol.25A, p.277-286, (1994).
11. O. Flores, L. Martinez, Journal of Materials Science, Vol.32, p.5985, (1997).
12. M. J. Luton, R. Darvel, R. A. Petkovic, Metall. Trans., p.411, (1980).
13. B. Dutta, C. M. Sellers, Mat. Sci. and Tech., Vol.3, p.197, (1987).
14. S.J. Wu, C.L. Davis; Journal of Microscopy, Vol.213, p.262-272, (2004).
15. D. Bhattacharjee, J.F. Knott, C.L. Davis; Metall. Trans, Vol.35A, p.121 (2004).
16. L. Zhang, C. L. Davis, M. Strangwood; 'Thermomechanical Processing of Steels', Vol. 2, Institute of Materials, London, 24 - 26 May, 2000, p. 764, (2000).
17. B. Mintz, J. R. Wilcox, D. N. Crowther, Mat. Sci. and Tech., Vol.2, p.589, (1986).
18. L. J. Cuddy, 'Thermomechanical Processing of Microalloyed Austenite', (edited by A. J. DeArdo, G. A. Ratz, P. J. Wray), T.M.S-A.S.M.E, Warrendale, Pa, p.129, (1982).
19. O. Known, A. J. DeArdo, Acta Metall. Mater., Vol.39, No.4, p.529, (1991).

TABLES

Table 2.1: Chemical compositions (wt%) of the as-cast slabs and rolled plate.

Sample	C	Si	Mn	P	S	Ni	Al	Nb	Ti	N	V
As-cast Slab 1	0.10	0.31	1.42	0.017	0.005	0.32	0.046	0.045	0.002	0.008	0.052
As-cast Slab 2	0.10	0.28	1.41	0.013	0.001	0.30	0.029	0.027	0.001	0.008	0.050
Rolled plate	0.09	0.34	1.53	0.014	0.003	0.28	0.046	0.041	0.004	0.007	0.09

Table 2.2: Heat treatment schedules for quarter thickness samples of as-cast slabs (all heating rates 1°C/min to 600°C, then 3°C/min to reheating temperature)

Sample	Reheating temperature and time	Cooling	Holding / Tempering
Slab1-1075-WQ-300	1075°C / 1 hr.	Ice-water quench to room temperature (RT)	Tempering at 300°C / 1 hr. Air cooled to RT
Slab1-1150-WQ-300	1150°C / 1 hr.		
Slab1-1225-WQ-300	1225°C / 1 hr		
Slab2-1150-WQ-300	1150°C / 1 hr		
Slab 1-1150-700-Hold	1150°C / 1 hr.	Quench to 700°C	Holding at 700°C / 1 hr. Air cooled to RT

Table 3.1: Average secondary dendritic arm spacing (SDAS) and ferrite grain size of the as-cast slabs.

	Average SDAS (μm)		ECD Ferrite grain size, (μm)	
Position	Slab 1	Slab 2	Slab 1	Slab 2
10 mm from top	92 ± 28	91 ± 26	50 ± 44	50 ± 47
30 mm from top	111 ± 27	113 ± 27	67 ± 56	70 ± 59
Quarter thickness	211 ± 36	198 ± 29	86 ± 62	89 ± 64
Mid-thickness	230 ± 38	231 ± 33	113 ± 84	102 ± 76

Table 3.2: Quantification of Al- and Nb-rich precipitate distributions in as-cast slab 1.

	Precipitate Area Density (Number/mm^2)			Interparticle Spacing (μm)	
	Minimum (Ppt-lean region)	Maximum (Ppt-rich region)	Average	Maximum (Ppt-lean region)	Minimum (Ppt-rich region)
Sub-surface (10 mm)	9×10^4	31×10^4	$(21\pm7)\times10^4$	3.13	0.87
¼-Thickness	12×10^4	60×10^4	$(41\pm14)\times10^4$	2.77	0.41
½-Thickness	8×10^4	74×10^4	$(43\pm19)\times10^4$	2.80	0.38

Table 3.3: Average ferrite grain size (Equivalent Circle Diameter, ECD) variation through thickness of the rolled plate sample.

	Sub-surface (5 mm from top)	Quarter-thickness (11 mm from top)	Mid-thickness (22 mm from top)
Average grain size (μm)	4.8 ± 3.7	6.3 ± 4.6	7.8 ± 6.7

TABLES

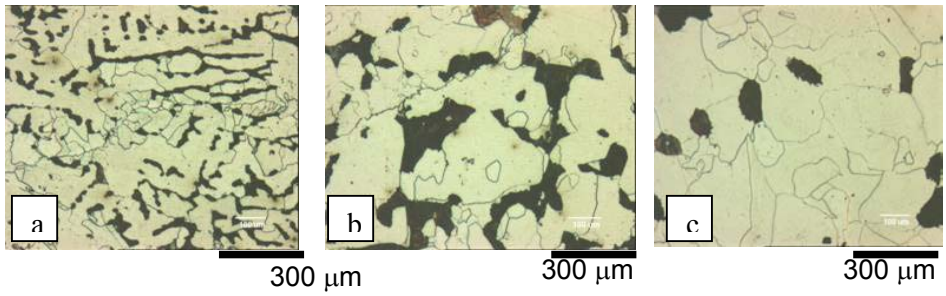

Fig. 3.1: Microstructure at (a) sub-surface (20 mm from top), (b) ¼-thickness and (c) mid-thickness of as-cast slab 1

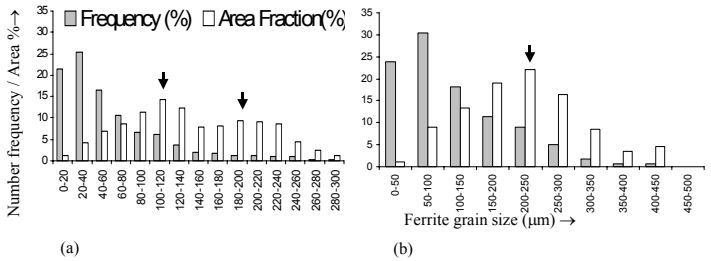

Fig. 3.2: Ferrite grain size distribution of as-cast slab 1 at (a) 20 mm from top surface, and (b) mid-

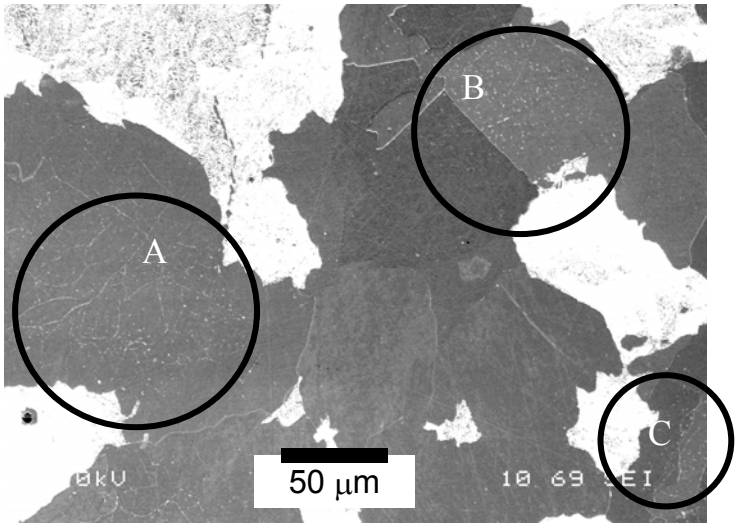

Fig.3.3: Inhomogeneous precipitate distribution in as-cast slab 1 with precipitate-rich regions, A, B

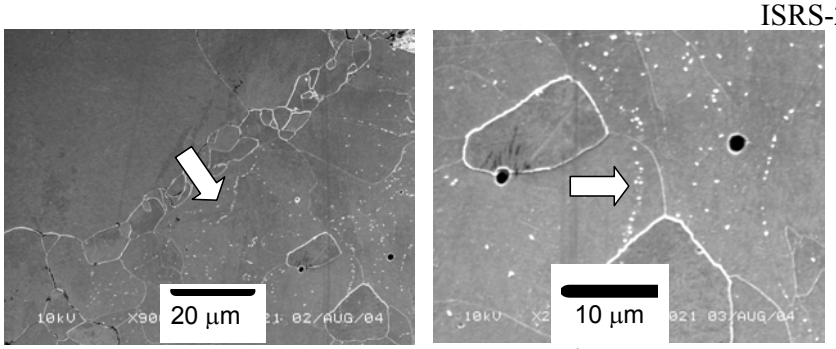

Fig.3.4: (a) Inhomogeneous precipitate distribution in as-cast slab 1 showing precipitate-rich regions (arrowed); and (b) cluster of precipitates in a precipitate-rich region.

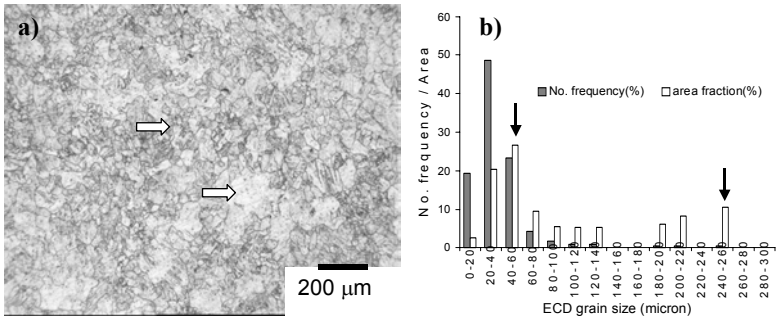

Fig.3.5: (a) Prior austenite grain structure in slab1-1150-WQ-300 sample. Coarse and fine grain regions are indicated by arrows; and (b) bimodality in austenite grain size distribution in the same sample.

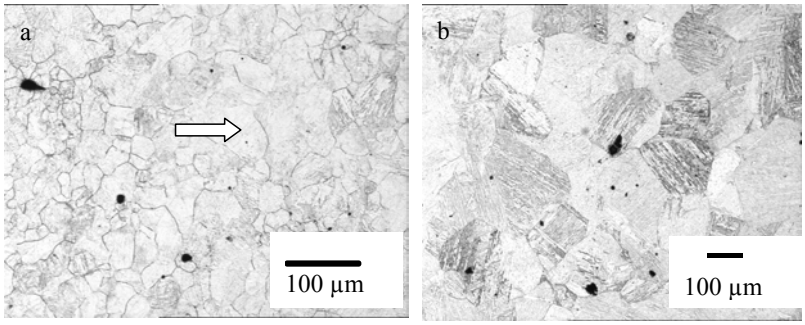

Fig.3.6: (a) Coarse grain regions (arrowed) in the bimodal austenite structure of slab2-1150-WQ-300 sample; and (b) uniform grain structure in slab1-1225-WQ-300 sample.

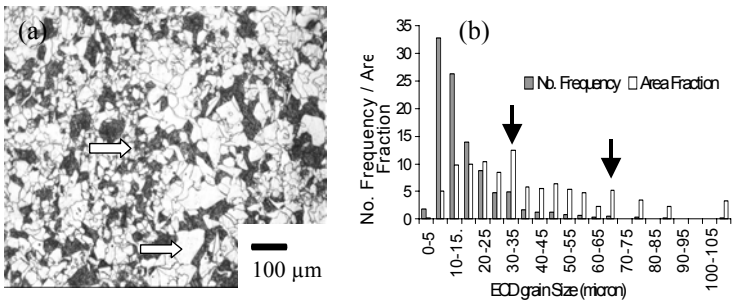

Fig.3.7: (a) Ferrite-pearlite structure with course and fine ferrite grains (arrowed) of slab1-1150-700-Hold sample; and (b) image analysis results showing the bimodality of ferrite grains

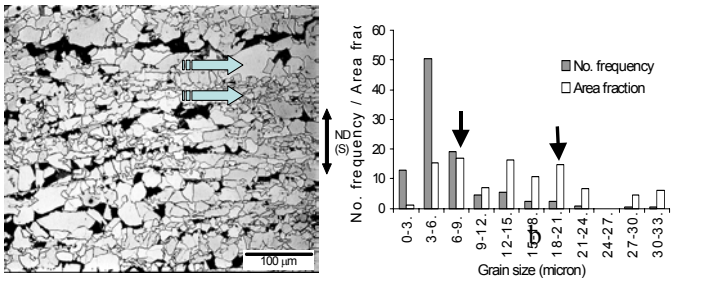

Fig.3.8: (a) Coarse and fine ferrite grains (arrowed) in ¼-thickness position of rolled steel sample. (b) Image analysis results showing the bimodality of ferrite grains.

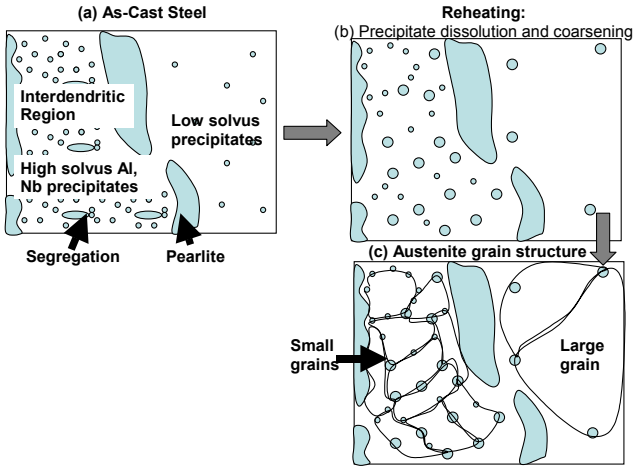

Fig.3.9: (a) Segregation of precipitates at interdendritic regions of as-cast steel; (b) precipitate dissolution and coarsening during reheating; and (c) formation of bimodal austenite structure due to the difference in pinning force.